Modelling the population-level protection conferred by COVID-19 vaccination

Pranesh Padmanabhan[1,*], Rajat Desikan[2,‡], Narendra M. Dixit[2,3,*]

[1]Clem Jones Centre for Ageing Dementia Research, Queensland Brain Institute, The University of Queensland, Brisbane, Australia 4072

[2]Department of Chemical Engineering, Indian Institute of Science, Bangalore, India 560012

[3]Centre for Biosystems Science and Engineering, Indian Institute of Science, Bangalore, India 560012

‡Current Address: Certara QSP, Certara UK Limited, Sheffield, UK

[*]**Correspondence:**

Pranesh Padmanabhan, Narendra M. Dixit

Email: p.padmanabhan@uq.edu.au; narendra@iisc.ac.in

One sentence summary:

Viremic control by the spectrum of neutralizing antibodies elicited by vaccination determines COVID-19 vaccine efficacies.

Manuscript details:

Abstract: 125 words; Text: ~2500 words; Figures: 4; References: 58 (30 in main text)

Supplementary Materials: Tables: 3; Figures: 5

Although severe acute respiratory syndrome coronavirus 2 (SARS-CoV-2) vaccines work predominantly by eliciting neutralizing antibodies (NAbs), how the protection they confer depends on the NAb response to vaccination is unclear. Here, we collated and analysed *in vitro* dose-response curves of >70 NAbs and constructed a landscape defining the spectrum of neutralization efficiencies of NAbs elicited. We mimicked responses of individuals by sampling NAb subsets of known sizes from the landscape and found that they recapitulated responses of convalescent patients. Combining individual responses with a mathematical model of within-host SARS-CoV-2 infection post-vaccination, we predicted how the population-level protection conferred would increase with the NAb response to vaccination. Our predictions captured the outcomes of vaccination trials. Our formalism may help optimize vaccination protocols, given limited vaccine availability.

Approved SARS-CoV-2 vaccines have shown remarkable but varying efficacies in clinical trials, reducing the incidence of symptomatic infections by 62-96% (*1-4*). The protection has been found to be predominantly due to NAbs elicited by the vaccines; cellular immunity appeared to play a secondary role (*1, 2*). The NAb response elicited by primary SARS-CoV-2 infection is diverse, spanning >1000-fold variation in Ab titres and *in vitro* neutralization efficiencies across individuals (*5, 6*), and appears not to correlate with disease severity (*7*). NAb titres following vaccination were comparable to or even lower at times than those from convalescent patients (*1, 2, 8*). The protection accorded by the vaccines is thus surprising. It is possible, based on animal studies (*9*), that lower NAb titres are protective at the time of challenge than post infection. Knowledge of how the level of protection depends on the

NAb titres and their neutralization efficiencies is lacking. This knowledge gap hinders rational optimization of vaccination protocols, which is important today given limited vaccine supplies (*10*). Here, we developed a mathematical model that quantitatively predicts the population-level protection conferred by vaccines as a function of the NAb responses they elicit.

A major challenge to describing the effects of vaccination is the diversity of the NAb responses elicited; no formalism exists to predict the diversity or its effects on protection. We addressed this challenge by adapting the classic idea of *shape space*, which has aided quantification of the immune repertoire (*11*), for characterizing NAbs. Accordingly, we sought features, also termed shape parameters, of the NAbs that would predict their neutralization efficiencies. Numerous studies have isolated individual NAbs from patients and assessed their neutralization efficiencies *in vitro*, with the aim of developing NAbs for therapeutic applications. We compiled dose-response curves (DRCs) of >70 NAbs thus isolated and fit them using the standard sigmoidal function as well as the median-effect equation (*12*) (materials and methods, fig. S1, table S1). The equations fit the data well (Fig. 1A, and figs. S2 and S3), indicating that two parameters, the 50% inhibitory concentration, IC_{50}, and the slope, m, of the DRC, were sufficient to characterize the neutralization efficiency of the NAbs (Fig. 1A and table S1). The best-fit IC_{50} and m varied widely across NAbs (Fig. 1B). IC_{50} ranged from ~10^{-3} µg/ml to ~140 µg/ml (Fig. 1B), in close agreement with reported estimates, giving us confidence in the fits (fig. S4A and table S1). m, the importance of which has been recognized with HIV-1 and hepatitis C (*12*, *13*) but has not typically been reported for SARS-CoV-2, spanned the range of ~0.2 to 2 (Fig. 1). This variability in IC_{50} and m was not restricted

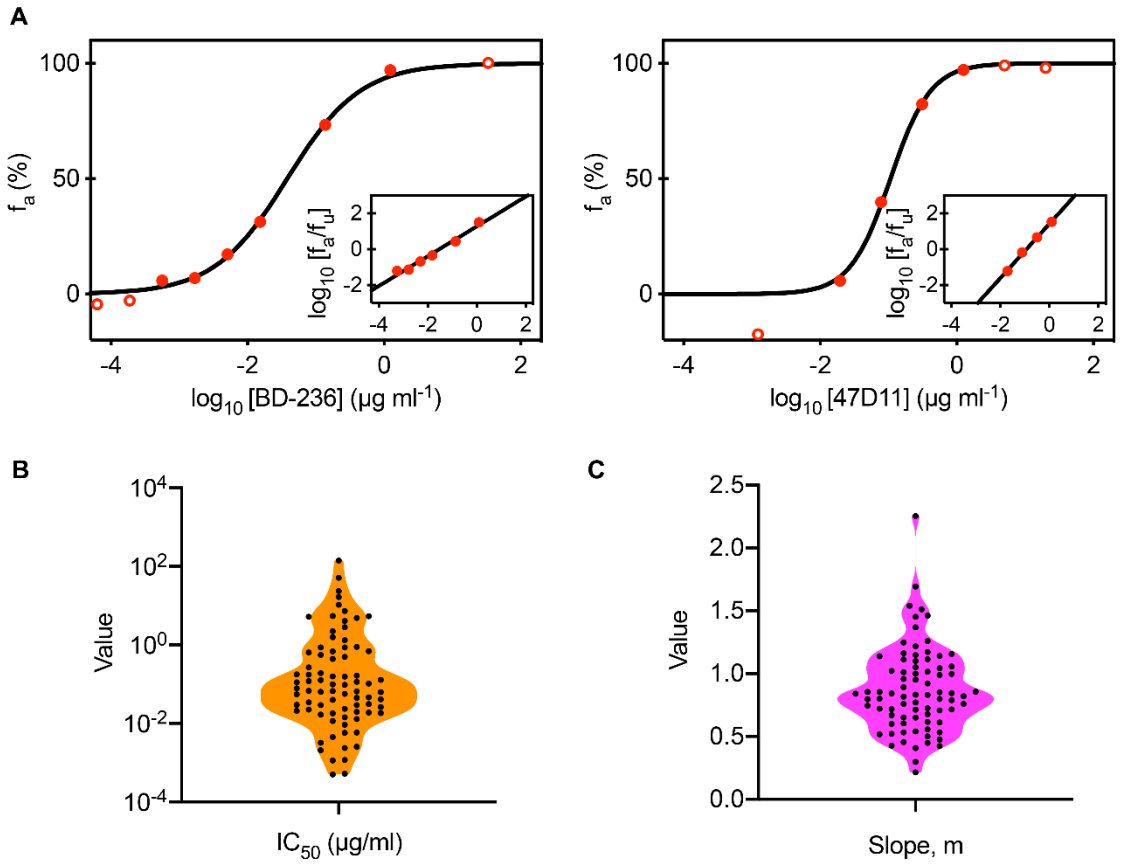

Figure 1. Analysis of dose-response curves of SARS-CoV-2 NAbs. (A) Fits (lines) of the standard sigmoidal equation and the median-effect equation (*inset*) to published experimental data (circles) of the fraction of infection events blocked, f_u, as a function of NAb concentration, shown for two NAbs, BD-236 (left) and 47D11 (right). Experimental data points with 1% < f_u < 99% (filled circles) were considered for parameter estimation. Fits for the remaining NAbs are in figs. S2 and S3. The best-fit estimates of (B) IC_{50} and (C) m for all the NAbs analysed.

to a particular pseudotyped virus construct or backbone used (fig. S4, B and C), the cell line used (fig. S4, D and E), or assay conditions, which could vary across studies (fig. S4, F and G). The variability was thus intrinsic to the NAbs, indicating the spectrum of NAbs elicited. Furthermore, akin to HIV-1 antibodies (*12*), the variations in IC_{50} and m of the SARS-CoV-2 NAbs appeared independent. For instance, the NAbs BD-361 and REGN10954 had similar IC_{50} (both ~0.04 µg/ml), but vastly different m (~0.7 and ~1.5, respectively), whereas the NAbs CC12.3 and 515-5 had vastly different IC_{50} (~0.02 µg/ml and 1.6 µg/ml, respectively), but

similar *m* (both ~1). IC_{50} and *m* were thus not only sufficient but also necessary for quantifying the neutralization efficiencies of NAbs. We therefore employed IC_{50} and *m* as the required shape parameters. Plotting the NAbs on an IC_{50}-*m* plot, we identified the NAb shape space (Fig. 2), which, because of its two-dimensional nature, we termed the 'landscape of SARS-CoV-2 NAbs'.

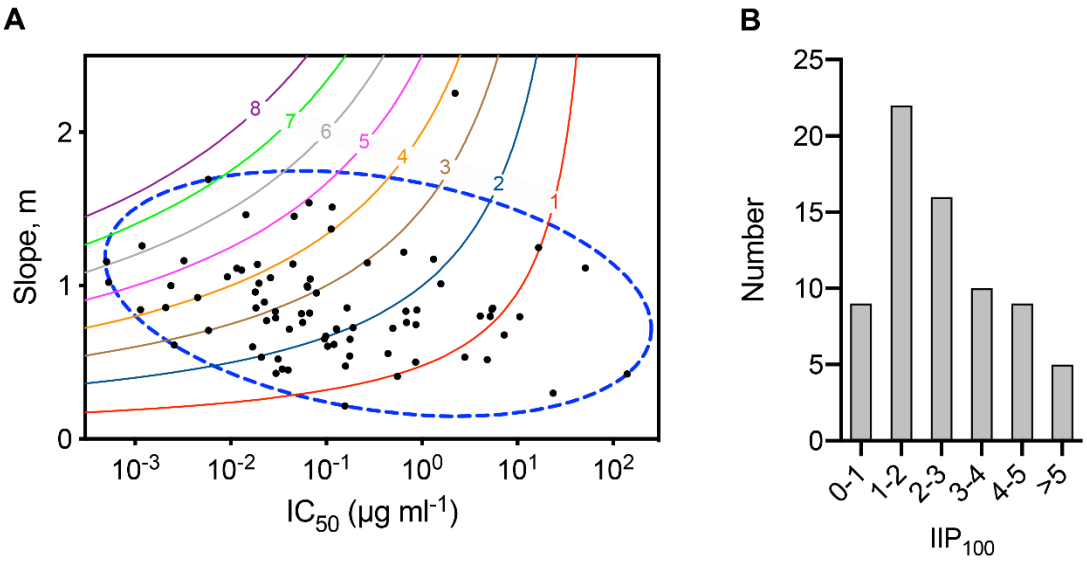

Figure 2. The landscape of SARS-CoV-2 NAbs. (A) SARS-CoV-2 NAbs analysed in Fig. 1 depicted on an IC_{50}-*m* plot. Each dot represents a NAb. 8 NAbs that have multiple neutralisation curves reported are represented multiple times (table S1). Solid lines are loci of points corresponding to fixed *IIP* values computed at 100 μg/ml. The ellipse (blue dashed line) circumscribes the landscape of SARS-CoV-2 NAbs elicited. (B) The distribution of IIP_{100} values of NAbs. Average IIP_{100} values are used for the 8 NAbs mentioned above.

The landscape contains potent NAbs, with low IC_{50} and high *m*, as well as weak NAbs, with the opposite traits. To compare the NAbs, we employed the instantaneous inhibitory potential (*IIP*), a composite metric of IC_{50} and *m* (*12-14*). IIP_D represents the $\log_{10}$ decline in viral load in a single round infection assay due to the NAb present at concentration *D*. Thus, the higher is the IIP_D, the more potent is the NAb at concentration *D*. NAbs displayed a wide distribution of IIP_{100} values (Fig. 2B and table S1): We found that 5 NAbs had the highest IIP_{100}

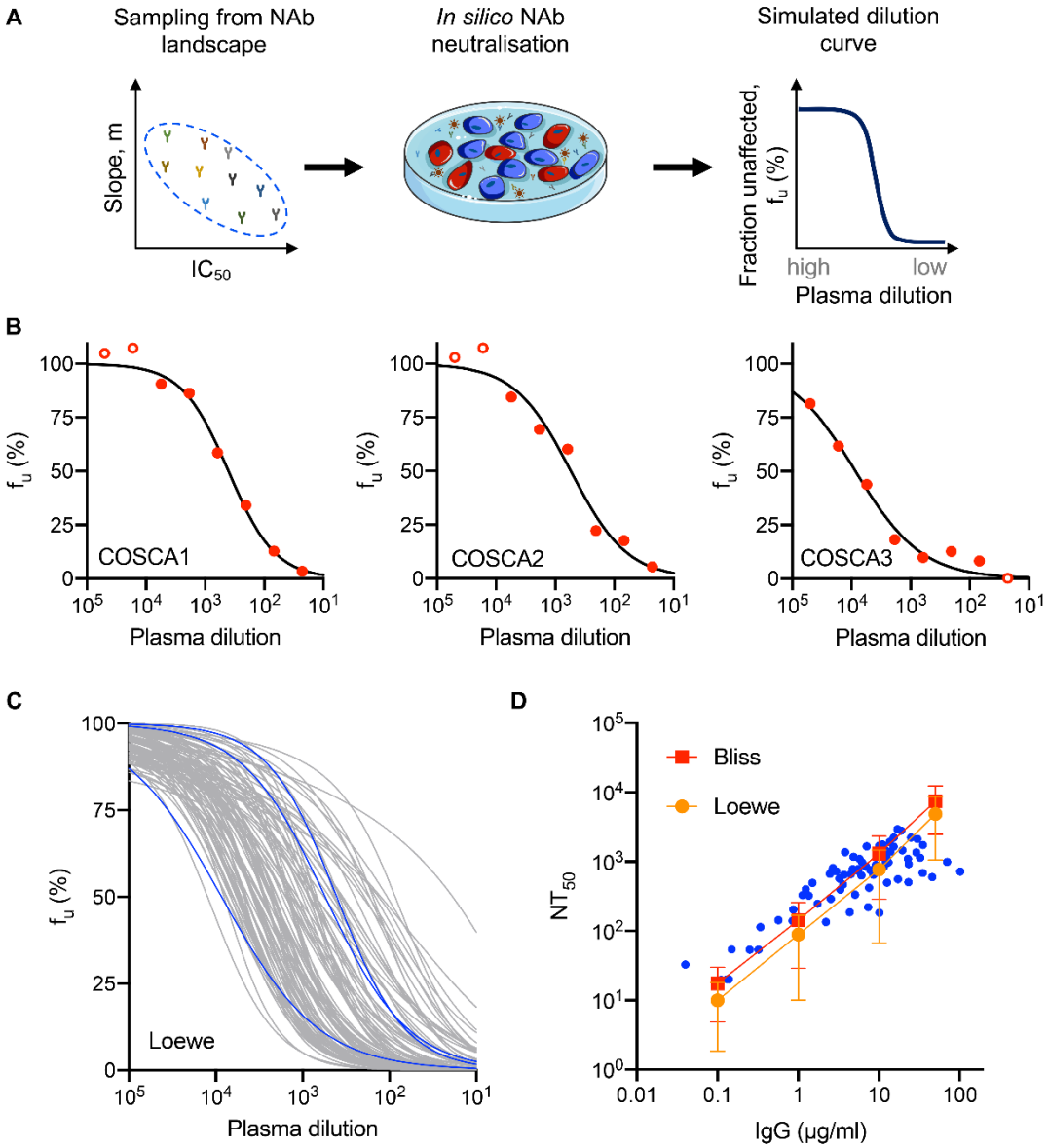

Figure 3. NAb landscape and patient responses. (A) Schematic of the procedure to predict plasma dilution curves. We represent an individual's plasma by a sample of NAbs from the landscape. We predict the fraction of infection events unaffected by NAbs, f_u, at a given plasma dilution in *in vitro* pseudovirus neutralization assays and repeat this at different dilutions to obtain the dilution curve. (B) Representative plasma dilution curves obtained as fits (lines) of the equation $f_u = \frac{(g)^n}{(g)^n + (NT_{50})^n}$ to reported data (circles) from three patients (*15*), where n is the Hill coefficient, γ is the plasma dilution and NT_{50} is the half-maximal inhibitory plasma neutralizing titre. Experimental data points with $1\% < f_u < 99\%$ (filled circles) were considered for parameter estimation. (C) Predictions (lines) of plasma dilution curves. We assumed ten NAbs per patient. Blue lines are fits shown in B. D_0 = 30 μg/ml. (D) Half-maximal inhibitory plasma neutralizing titre, NT_{50}, as a function of total NAb concentration. Blues circles are reported estimates from convalescent patients. Red squares and orange circles are the mean of NT_{50} values predicted from 100 virtual patients at each NAb concentration using Bliss independence and Loewe additivity, respectively. The error bars are standard deviations.

values, >5, and 9 had the least, <1 (D = 100 µg/mL) (Fig. 2B and table S1). This distribution of IIP_{100} values demonstrated further the wide spectrum of neutralization efficiencies of NAbs.

The landscape established bounds on the neutralization efficiencies of the NAbs elicited. We reasoned next that the diversity of the NAb responses across individuals would arise from the way NAbs are sampled from the landscape. Although a large number of NAbs can be isolated from individuals, studies of convalescent patient plasma (*5*, *6*, *16*-*18*) as well as on NAb epitope profiling (*19*) have argued that the NAb response of an individual can be attributed to a small subset of 5-10 distinct NAbs. Furthermore, while some epitopes on the SARS-CoV-2 spike protein, S, are targeted more than others by NAbs, the collection of NAbs produced differs substantially across individuals (*20*). We therefore assumed that the response elicited by an infected individual would be a *small*, *random subset* of the landscape. We analysed DRCs of NAbs isolated from individual patients and found that they indeed constituted such random subsets in the landscape (fig. S5). Accordingly, we sampled random combinations of 10 NAbs each, each combination representing the response of an individual. We let NAb concentrations vary across individuals, to mimic the observed variation of the NAb titres (*16*-*18*). We quantified the neutralization efficiency of the NAb response by simulating standard plasma dilution assays (materials and methods, Fig. 3A). We let the NAbs exhibit Bliss independence or Loewe additivity, the former representing NAbs targeting distinct, non-occluding epitopes and the latter the same or occluding epitopes (*21*). Our simulations recapitulated the dilution curves associated with patient plasma (Fig. 3, B and C). The values of NT_{50}, the dilution at which the neutralization efficiency of the plasma decreases by 50%, were in agreement with experimental observations (*17*) (Fig. 3D). The data was described better by Bliss independence

at low NAb titres and Loewe additivity at high titres. This is expected because at low titres, the NAbs are unlikely to interact with each other and would thus follow Bliss independence, whereas at high titres, they may compete for binding sites on S or occlude each other and thus exhibit Loewe additivity (*21*). At any NAb titre, there existed substantial variation in NT_{50}, attributed to the random combinations of NAbs sampled. The variation, however, was outweighed by the overall rise of NT_{50} with the NAb titre, consistent with patient data (Fig. 3D). For instance, the NT_{50} was 17±13 at the IgG titre of 0.1 µg/ml and 1300±1000 at 10 µg/ml. Sampling from the NAb landscape thus successfully recapitulated patient responses. We were able to describe the diversity of the NAb responses elicited across patients. Armed with this description, we examined next the protection accorded by vaccines in clinical trials.

Following vaccination, NAb titres rise and are expected to remain stable (or decay slowly) over weeks to months (*22*), protecting individuals who might get exposed to the virus during this period. Individuals were assumed to be protected if they did not report symptomatic infection; loss of protection involved symptoms and a positive result on a nucleic acid amplification test (*1*, *2*). Protection with NAbs is expected not to be sterilizing, as suggested by animal studies (*9*); NAbs help suppress the peak in viremia, thereby reducing symptoms, and facilitate more rapid clearance of the infection. If the peak is sufficiently suppressed, no symptoms may result, as is the case with the ~40% of natural infections that remain asymptomatic (*7*). Here, we assumed that an individual would be detected as symptomatically infected if the viral load rose above a threshold during the infection.

To estimate the peak viral load, we developed a mathematical model of the early time course of the infection, where the viral load typically rises, attains a peak, and declines (*23*),

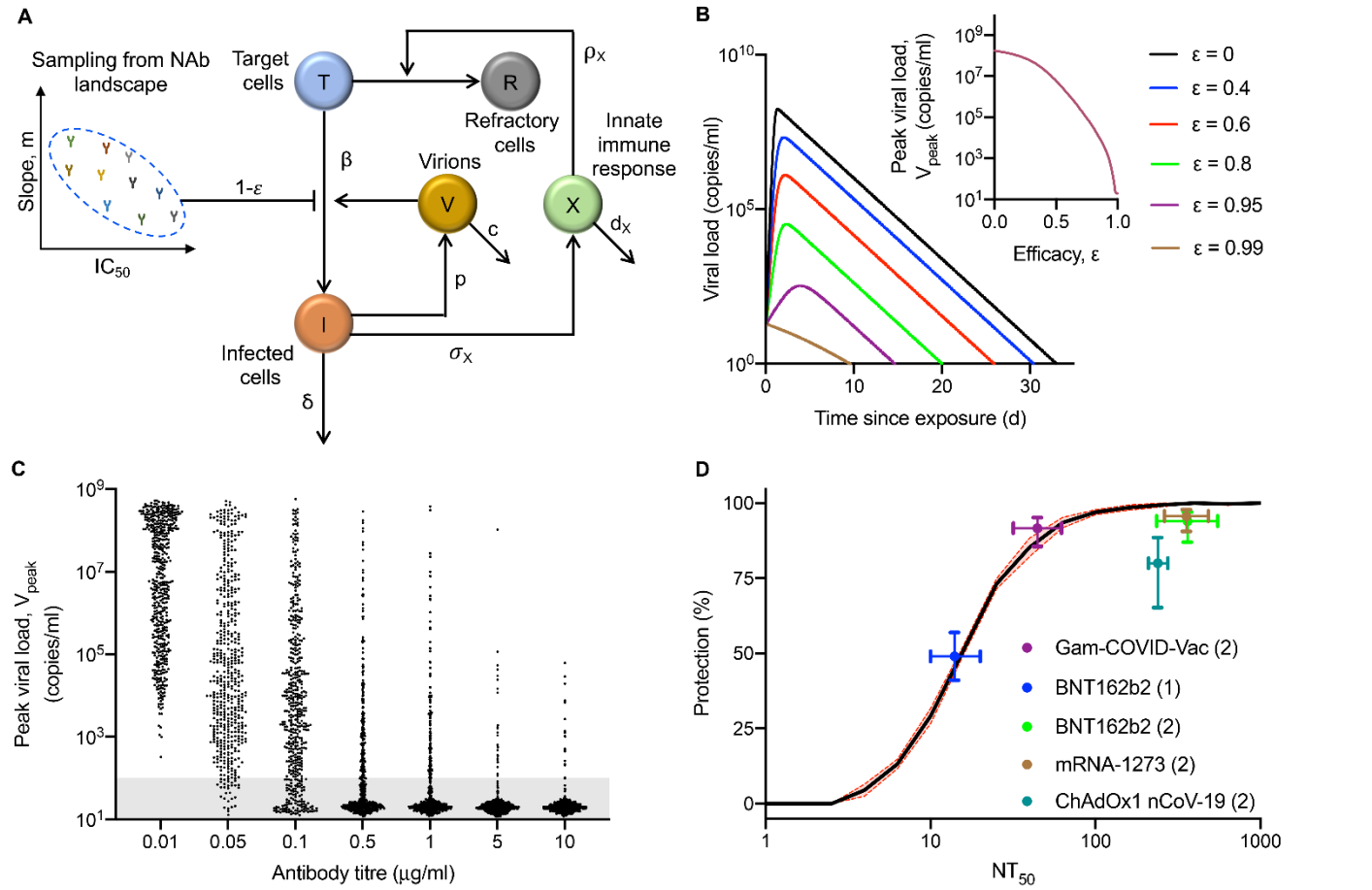

Figure 4. SARS-CoV-2 dynamics and protection post-vaccination. (A) Schematic of the model of within-host SARS-CoV-2 dynamics post-vaccination depicting the interactions between target cells, *T*, infected cells, *I*, refractory cells, *R*, virions, *V*, innate immune response, *X*, and pre-existing NAbs, sampled from the landscape. (B) Predictions of viral load in non-vaccinated (black line) and vaccinated (coloured lines) individuals with different fixed efficacies of NAbs indicated. *Inset*: Predicted peak viral load at different efficacies. (C) Predictions of peak viral load at different NAb titres. Each dot represents a patient. (D) Model predictions of the relationship between mean protection and NT_{50} (solid line) compared with data from vaccination trial (symbols). The number of doses of the vaccine administered is mentioned in brackets. The error bars (dashed lines) in the protection curve are the standard deviation from 5 realizations of *in silico* patient populations. The data from the trials used is summarized in table S3. The model equations and simulation procedure are described in materials and methods.

and applied it to describe the effect of vaccination (Fig. 4A, table S2, materials and methods). The structure of the model mimics recent models that have captured patient data of viral load changes following primary infection (*24, 25*) (see Fig. 4B, ε=0). In addition, we assumed that

NAbs generated following vaccination would exist at the start of infection and neutralize free viruses, effectively reducing viral infectivity. The greater the reduction in infectivity, the lower the peak viral load (Fig. 4B, $\varepsilon>0$). Significant *de novo* NAb production post-infection typically occurs after the peak in viremia (*7*). We therefore considered pre-existing NAbs as responsible for protection and assumed their titres not to vary substantially during the course of the infection, given the typically short course of the infection and the much longer durability of the NAb response to vaccination (*22*). (Our model is not applicable to natural infection before vaccination; no models are currently capable of correctly describing NAb responses following primary infection.) We let the pre-existing NAbs be drawn as random subsets from the landscape, as we did above. The NAbs neutralized free viruses with an efficiency that we estimated using Loewe additivity between the individual NAbs (Fig. 4). NAb titres in the lung airways are expected to be similar to those in the blood given the close coupling between the lungs and the circulatory system (*7*). We simulated a virtual patient population of 3500 individuals, on the order of the number of individuals infected in the placebo arms of clinical trials. The individuals all had distinct viral dynamics parameters drawn from known ranges (table S2), to mimic interpatient variability in addition to the variability arising from NAb sampling from the landscape. Our model predicted wide variability in the peak viral load (Fig. 4C). At low pre-existing NAb concentrations (0.01 μg/mL), indicative of the scenario without vaccination, the predicted peak viral load ranged from ~10^3 to 10^9 copies/ml, consistent with the range in symptomatic individuals (*26*). The peaks declined as NAb titres increased. The limit of detection is ~10^2 copies/ml (*27*), which we set as the threshold for symptomatic

infection that would be detected in trials. The fraction of individuals with peaks below detection would indicate the level of protection due to the vaccine.

To quantify the mean level of protection and test it against data from clinical trials, we used viral dynamics parameters representative of symptomatic infections (*24*, *25*) (table S2) and simulated the dynamics in 5 cohorts of 2000 infected individuals each. Vaccination studies report the NT_{50} values of the NAb responses elicited and the associated mean protection level, or efficacy (table S3). We binned the different individuals into narrow NT_{50} bands and calculated the mean protection in each band. We found that the mean protection was low for NT_{50}~1. It increased in a sigmoidal manner to 50% at NT_{50}~20 and asymptotically reached 100% at NT_{50}~200. Remarkably, the data for nearly all approved vaccines fell on this 'protection curve', explaining the protection they confer (Fig. 4D). Thus, for instance, a single dose of the vaccine BNT 162b2 elicited NAbs with NT_{50} of 14 and accorded 49% protection. Following two doses, the corresponding values were 361 and 94%, respectively. These values as well as those for other vaccines were captured accurately by our model predictions. The only exception was ChAdOx1 nCoV-19, which had a lower protection than predicted, the reasons for which remain to be elucidated.

Our study provides the first conceptual, mechanistic and quantitative understanding of the protection conferred by COVID-19 vaccines. Our findings would inform strategies for optimal vaccine deployment. With limited vaccine availability, it would be useful to estimate the protection realizable by a single dose of a prime-boost vaccine, especially in younger, less vulnerable adults (*10*). Our formalism would enable this estimation: measurements of corresponding NT_{50} values would allow reading off the expected protection levels from our

protection curve. Similarly, using measurements of the waning of NAb titres post-vaccination, how the population-level protection due to pre-existing NAbs would fade could be predicted. Protection would then rely on memory B cell responses, which are yet to be fully understood (*28*), or indicate the need for revaccination. Our study did not consider viral mutations because with 5-10 NAbs active, viral escape from NAb responses is expected to be unlikely (*19*, *29*). With the new circulating strains (*30*), however, the NAb landscape may have to be reconstructed. Future studies may report DRCs of NAbs against the new strains, facilitating such reconstruction.

References

1. L. R. Baden *et al.*, Efficacy and safety of the mRNA-1273 SARS-CoV-2 vaccine. *N Engl J Med* **384**, 403-416 (2021).
2. F. P. Polack *et al.*, Safety and efficacy of the BNT162b2 mRNA COVID-19 vaccine. *N Engl J Med* **383**, 2603-2615 (2020).
3. M. Voysey *et al.*, Safety and efficacy of the ChAdOx1 nCoV-19 vaccine (AZD1222) against SARS-CoV-2: an interim analysis of four randomised controlled trials in Brazil, South Africa, and the UK. *Lancet* **397**, 99-111 (2021).
4. D. Y. Logunov *et al.*, Safety and efficacy of an rAd26 and rAd5 vector-based heterologous prime-boost COVID-19 vaccine: an interim analysis of a randomised controlled phase 3 trial in Russia. *Lancet* **397**, 671-681 (2021).
5. L. Liu *et al.*, Potent neutralizing antibodies against multiple epitopes on SARS-CoV-2 spike. *Nature* **584**, 450-456 (2020).
6. D. F. Robbiani *et al.*, Convergent antibody responses to SARS-CoV-2 in convalescent individuals. *Nature* **584**, 437-442 (2020).
7. A. Sette, S. Crotty, Adaptive immunity to SARS-CoV-2 and COVID-19. *Cell* **184**, 861-880 (2021).

8. P. M. Folegatti *et al.*, Safety and immunogenicity of the ChAdOx1 nCoV-19 vaccine against SARS-CoV-2: a preliminary report of a phase 1/2, single-blind, randomised controlled trial. *Lancet* **396**, 467-478 (2020).

9. K. McMahan *et al.*, Correlates of protection against SARS-CoV-2 in rhesus macaques. *Nature* **590**, 630-634 (2021).

10. K. M. Bubar *et al.*, Model-informed COVID-19 vaccine prioritization strategies by age and serostatus. *Science* **371**, 916-921 (2021).

11. A. S. Perelson, G. F. Oster, Theoretical studies of clonal selection: Minimal antibody repertoire size and reliability of self-non-self discrimination. *J Theor Biol* **81**, 645-670 (1979).

12. N. E. Webb, D. C. Montefiori, B. Lee, Dose-response curve slope helps predict therapeutic potency and breadth of HIV broadly neutralizing antibodies. *Nat Commun* **6**, 8443 (2015).

13. P. Padmanabhan, N. M. Dixit, Inhibitors of hepatitis C virus entry may be potent ingredients of optimal drug combinations. *Proc Natl Acad Sci U S A* **114**, E4524-E4526 (2017).

14. B. L. Jilek *et al.*, A quantitative basis for antiretroviral therapy for HIV-1 infection. *Nat Med* **18**, 446-451 (2012).

15. P. J. M. Brouwer *et al.*, Potent neutralizing antibodies from COVID-19 patients define multiple targets of vulnerability. *Science* **369**, 643-650 (2020).

16. B. Isho *et al.*, Persistence of serum and saliva antibody responses to SARS-CoV-2 spike antigens in COVID-19 patients. *Sci Immunol* **5**, eabe5511 (2020).

17. A. S. Iyer *et al.*, Persistence and decay of human antibody responses to the receptor binding domain of SARS-CoV-2 spike protein in COVID-19 patients. *Sci Immunol* **5**, eabe0367 (2020).

18. K. Röltgen *et al.*, Defining the features and duration of antibody responses to SARS-CoV-2 infection associated with disease severity and outcome. *Sci Immunol* **5**, eabe0240 (2020).

19. E. Shrock *et al.*, Viral epitope profiling of COVID-19 patients reveals cross-reactivity and correlates of severity. *Science* **370**, eabd4250 (2020).

20. M. Yuan *et al.*, Structural basis of a shared antibody response to SARS-CoV-2. *Science* **369**, 1119-1123 (2020).

21. C. T. Meyer *et al.*, Quantifying drug combination synergy along potency and efficacy axes. *Cell Systems* **8**, 97-108.e116 (2019).

22. A. T. Widge *et al.*, Durability of responses after SARS-CoV-2 mRNA-1273 vaccination. *N Engl J Med* **384**, 80-82 (2021).

23. R. Wölfel *et al.*, Virological assessment of hospitalized patients with COVID-2019. *Nature* **581**, 465-469 (2020).

24. A. Goyal, E. F. Cardozo-Ojeda, J. T. Schiffer, Potency and timing of antiviral therapy as determinants of duration of SARS-CoV-2 shedding and intensity of inflammatory response. *Sci Adv* **6**, eabc7112 (2020).

25. A. Gonçalves *et al.*, Timing of antiviral treatment initiation is critical to reduce SARS-CoV-2 viral load. *CPT: Pharmacometrics & Systems Pharmacology* **9**, 509-514 (2020).

26. J. Fajnzylber *et al.*, SARS-CoV-2 viral load is associated with increased disease severity and mortality. *Nat Commun* **11**, 5493 (2020).

27. R. Arnaout *et al.*, SARS-CoV2 testing: the limit of detection matters. *bioRxiv* 10.1101/2020.1106.1102.131144 (2020).

28. R. R. Goel *et al.*, Longitudinal analysis reveals distinct antibody and memory B cell responses in SARS-CoV2 naïve and recovered individuals following mRNA vaccination. *medRxiv* 10.1101/2021.1103.1103.21252872 (2021).

29. A. Baum *et al.*, Antibody cocktail to SARS-CoV-2 spike protein prevents rapid mutational escape seen with individual antibodies. *Science* **369**, 1014-1018 (2020).

30. T. C. Williams, W. A. Burgers, SARS-CoV-2 evolution and vaccines: cause for concern? *Lancet Respiratory Medicine* 10.1016/S2213-2600(1021)00075-00078 (2021).

31. X. Chi *et al.*, A neutralizing human antibody binds to the N-terminal domain of the Spike protein of SARS-CoV-2. *Science* **369**, 650-655 (2020).

32. C. Wang *et al.*, A human monoclonal antibody blocking SARS-CoV-2 infection. *Nat Commun* **11**, 2251 (2020).

33. E. Seydoux *et al.*, Analysis of a SARS-CoV-2-infected individual reveals development of potent neutralizing antibodies with limited somatic mutation. *Immunity* **53**, 98-105 e105 (2020).

34. R. Shi *et al.*, A human neutralizing antibody targets the receptor-binding site of SARS-CoV-2. *Nature* **584**, 120-124 (2020).

35. A. Z. Wec *et al.*, Broad neutralization of SARS-related viruses by human monoclonal antibodies. *Science* **369**, 731-736 (2020).

36. C. Lei *et al.*, Neutralization of SARS-CoV-2 spike pseudotyped virus by recombinant ACE2-Ig. *Nat Commun* **11**, 2070 (2020).

37. Z. Lv *et al.*, Structural basis for neutralization of SARS-CoV-2 and SARS-CoV by a potent therapeutic antibody. *Science* **369**, 1505-1509 (2020).

38. S. J. Zost *et al.*, Potently neutralizing and protective human antibodies against SARS-CoV-2. *Nature* **584**, 443-449 (2020).

39. B. Ju *et al.*, Human neutralizing antibodies elicited by SARS-CoV-2 infection. *Nature* **584**, 115-119 (2020).

40. Y. Cao *et al.*, Potent neutralizing antibodies against SARS-CoV-2 identified by high-throughput single-cell sequencing of convalescent patients' B cells. *Cell* **182**, 73-84 e16 (2020).

41. J. Hansen *et al.*, Studies in humanized mice and convalescent humans yield a SARS-CoV-2 antibody cocktail. *Science* **369**, 1010-1014 (2020).

42. T. F. Rogers *et al.*, Isolation of potent SARS-CoV-2 neutralizing antibodies and protection from disease in a small animal model. *Science* **369**, 956-963 (2020).

43. C. O. Barnes *et al.*, Structures of human antibodies bound to SARS-CoV-2 spike reveal common epitopes and recurrent features of antibodies. *Cell* **182**, 828-842 e816 (2020).

44. D. Pinto *et al.*, Cross-neutralization of SARS-CoV-2 by a human monoclonal SARS-CoV antibody. *Nature* **583**, 290-295 (2020).

45. L. Hanke *et al.*, An alpaca nanobody neutralizes SARS-CoV-2 by blocking receptor interaction. *Nat Commun* **11**, 4420 (2020).

46. X. Chen *et al.*, Human monoclonal antibodies block the binding of SARS-CoV-2 spike protein to angiotensin converting enzyme 2 receptor. *Cell Mol Immunol* **17**, 647-649 (2020).

47. J. Wan *et al.*, Human-IgG-neutralizing monoclonal antibodies block the SARS-CoV-2 infection. *Cell Rep* **32**, 107918 (2020).

48. P. Padmanabhan, N. M. Dixit, Modeling suggests a mechanism of synergy between hepatitis C virus entry inhibitors and drugs of other classes. *CPT Pharmacometrics Syst Pharmacol* **4**, 445-453 (2015).

49. T. C. Chou, Theoretical basis, experimental design, and computerized simulation of synergism and antagonism in drug combination studies. *Pharmacol Rev* **58**, 621-681 (2006).

50. P. Padmanabhan, R. Desikan, N. M. Dixit, Targeting TMPRSS2 and Cathepsin B/L together may be synergistic against SARS-CoV-2 infection. *PLoS Comput Biol* **16**, e1008461 (2020).

347 51. V. I. Zarnitsyna *et al.*, Mathematical model reveals the role of memory CD8 T cell
348 populations in recall responses to Influenza. *Front Immunol* **7**, 165 (2016).

349 52. R. Ke, C. Zitzmann, R. M. Ribeiro, A. S. Perelson, Kinetics of SARS-CoV-2 infection in
350 the human upper and lower respiratory tracts and their relationship with infectiousness.
351 *medRxiv* 10.1101/2020.1109.1125.20201772 (2020).

352 53. D. A. Swan *et al.*, Vaccines that prevent SARS-CoV-2 transmission may prevent or dampen
353 a spring wave of COVID-19 cases and deaths in 2021. *medRxiv*
354 10.1101/2020.1112.1113.20248120 (2020).

355 54. A. S. Perelson, R. Ke, Mechanistic modeling of SARS-CoV-2 and other infectious diseases
356 and the effects of therapeutics. *Clin Pharmacol Ther* 10.1002/cpt.2160 (2020).

357 55. N. Dagan *et al.*, BNT162b2 mRNA COVID-19 vaccine in a nationwide mass vaccination
358 setting. *N Engl J Med*, 10.1056/NEJMoa2101765 (2021).

359 56. E. E. Walsh *et al.*, Safety and immunogenicity of two RNA-Based COVID-19 vaccine
360 candidates. *N Engl J Med* **383**, 2439-2450 (2020).

361 57. E. J. Anderson *et al.*, Safety and immunogenicity of SARS-CoV-2 mRNA-1273 vaccine in
362 older adults. *N Engl J Med* **383**, 2427-2438 (2020).

363 58. M. Voysey *et al.*, Single-dose administration and the influence of the timing of the booster
364 dose on immunogenicity and efficacy of ChAdOx1 nCoV-19 (AZD1222) vaccine: a pooled
365 analysis of four randomised trials. *Lancet* **397**, 881-891 (2021).

366

367

Acknowledgements

Funding: This work was supported by the DBT/Wellcome Trust India Alliance Senior Fellowship IA/S/14/1/501307 to NMD. **Author contributions:** PP: Conceptualization, Investigation, Formal analysis, Writing-original draft, Writing-review & editing; RD: Formal analysis, Writing-review & editing. NMD: Conceptualization, Writing-original draft, Writing-review & editing. **Competing interests:** The authors declare that no conflicts of interests exist. **Data and materials availability:** All relevant data are available within the manuscript and supplementary materials.